

Document downloaded from:

<http://hdl.handle.net/10251/70076>

This paper must be cited as:

Zwart, MP.; Pijlman, G.; Sardanyes Cayuela, J.; Duarte, J.; Januario, C.; Elena Fito, SF. (2013). Complex dynamics of defective interfering baculoviruses during serial passage in insect cells. *Journal of Biological Physics*. 39(2):327-342. doi:10.1007/s10867-013-9317-9.



The final publication is available at

<http://dx.doi.org/10.1007/s10867-013-9317-9>

Copyright Springer Verlag (Germany)

Additional Information

# Complex dynamics of defective interfering baculoviruses during serial passage in insect cells

Mark P. Zwart<sup>a,b\*</sup>, Gorben P. Pijlman<sup>c</sup>, Josep Sardanyés<sup>d,e</sup>, Jorge Duarte<sup>f,g</sup>, Cristina Januário<sup>f</sup>, and Santiago F. Elena<sup>a,h</sup>

<sup>a</sup> Instituto de Biología Molecular y Celular de Plantas, Consejo Superior de Investigaciones Científicas-UPV, València, Spain

<sup>b</sup> Quantitative Veterinary Epidemiology Group, Wageningen University, The Netherlands

<sup>c</sup> Laboratory of Virology, Wageningen University, The Netherlands.

<sup>d</sup> ICREA-Complex Systems Laboratory, Universitat Pompeu Fabra, Barcelona, Spain

<sup>e</sup> Institut de Biologia Evolutiva (CSIC-Universitat Pompeu Fabra), Barcelona, Spain

<sup>f</sup> Engineering Superior Institute of Lisbon, Lisboa, Portugal.

<sup>g</sup> Centro de Análise Matemática, Geometria e Sistemas Dinâmicos, Instituto Superior Técnico, Lisboa, Portugal.

<sup>h</sup> The Santa Fe Institute, Santa Fe, NM 87501, USA

\*Corresponding author:

Instituto de Biología Molecular y Celular de Plantas, Consejo Superior de Investigaciones Científicas-UPV, CL Ingeniero Fausto Elio s/n, 46022 Valencia, Spain

Tel: 34 963 877009 ext. 78368 or 34 618883996

Fax: 34 963 877859

Email addresses: [marzwa@upvnet.upv.es](mailto:marzwa@upvnet.upv.es)

1 **Abstract**

2 Defective interfering (DI) viruses are thought to cause oscillations in virus levels, known as  
3 the “Von Magnus effect”. Interference by DI viruses has been proposed to underlie these  
4 dynamics, although experimental tests of this idea have not been forthcoming. For the  
5 baculoviruses, insect viruses commonly used for the expression of heterologous proteins in  
6 insect cells, the molecular mechanisms underlying DI generation have been investigated.  
7 However, the dynamics of baculovirus populations harboring DIs have not been studied in  
8 detail. In order to address this issue, we used quantitative real-time PCR to determine the  
9 levels of helper and DI viruses during 50 serial passages of *Autographa californica* multiple  
10 nucleopolyhedrovirus (AcMNPV) in Sf21 cells. Unexpectedly, the helper and DI viruses  
11 changed levels largely in phase, and oscillations were highly irregular, suggesting the  
12 presence of chaos. We therefore developed a simple mathematical model of baculovirus-DI  
13 dynamics. This theoretical model reproduced patterns qualitatively similar to the  
14 experimental data. Although we cannot exclude that experimental variation (noise) plays an  
15 important role in generating the observed patterns, the presence of chaos in the model  
16 dynamics was confirmed with the computation of the maximal Lyapunov exponent, and a  
17 Ruelle-Takens-Newhouse route to chaos was identified at decreasing production of DI  
18 viruses, using mutation as a control parameter. Our results contribute to a better  
19 understanding of the dynamics of DI baculoviruses, and suggest that changes in virus levels  
20 over passages may exhibit chaos.

21

22 **Keywords:** baculovirus, bifurcations, chaos, defective interfering virus, experimental  
23 evolution

24

## 25 **1 Introduction**

26

27 Defective interfering (DI) viruses were first reported by Von Magnus [1], who studied their  
28 development in *Influenza A virus* populations passaged in embryonated chicken eggs.  
29 Based on these serial passage experiments the existence of ‘incomplete’ virus variants  
30 which increase rapidly in frequency and cause drops in overall virus titers was proposed.  
31 The existence of virus variants with large genomic deletions has since been confirmed in  
32 many virus families [2], including the Alphabaculoviruses [3,4]. DI viruses are generated  
33 almost instantly and accumulate rapidly when baculoviruses are introduced into cultured  
34 insect cells [5,6], leading to problems with sustained expression of heterologous proteins [3]  
35 in this widely used expression system [7]. DI viruses are thought to replicate much faster  
36 than viruses with a full-length genome, due to their smaller genome sizes. Moreover, DIs  
37 can evolve other strategies to better compete with helper viruses, such as the accumulation  
38 of origins of DNA replication within a single genome [8-10], a phenomenon that can be cell-  
39 line dependent [11]. On the other hand, DI viruses cannot autonomously replicate because  
40 they lack essential genes. DI viruses must therefore co-infect a cell with a helper virus in  
41 order to replicate, becoming obligate parasites of helper viruses, as they must co-opt gene  
42 products and cannot replicate on their own. When the frequency of the DI virus is high,  
43 overall virus production is low because essential gene products – which must come from a  
44 helper virus – are no longer available (i.e., interference). DI viruses can have implications for  
45 virus amplification in cultured cells, protein expression using viral vectors, and vaccination  
46 [12].

47 Co-existence of DI and helper viruses is thought to lead to regular cyclical changes in  
48 virus titer: there is a repeated decrease followed by an increase in virus titers over passages.  
49 These cyclical changes have been observed in many viral systems [2,13-16] and have been  
50 dubbed the “Von Magnus effect”. The following mechanism [2] has been suggested to

51 account for these fluctuations in virus titer: (i) cells are infected with a virus population  
52 composed of a helper and a DI virus, or a DI virus is generated spontaneously by mutation,  
53 (ii) virus amplification leads to an increase in the cellular multiplicity of infection, the number  
54 of virions infecting each cell, (iii) the DI virus will eventually reach a higher frequency of  
55 occurrence than the helper virus, as it has a selective advantage over the helper virus during  
56 cellular co-infection, and (iv) when the frequency of the DI virus becomes high, interference  
57 occurs and the titers of both viruses drop. The process then repeats itself, resulting in  
58 cyclical fluctuations in virus titers.

59 There is some experimental evidence that this mechanism is important for generating  
60 cyclical changes in virus titer. Palma and Huang [16] tracked the titer of helper and DI  
61 *Vesicular stomatitis virus* (VSV) variants and found that the two viruses evolved out of phase.  
62 Kawai *et al.* [14] showed that VSV plaque-forming units peak before viral capsid inclusions –  
63 an indicator of DI presence – accumulate in cells. On the other hand, Stauffer Thompson  
64 and Yin [17] observed irregular fluctuations of VSV over passages in the presence of DI  
65 viruses, which were attributed to experimental variation in available cellular resources. The  
66 idea that the dynamics of DI viruses could lead to irregular patterns had, however, already  
67 been made previously based on theoretical work, albeit for different reasons. Deterministic  
68 mathematical models of defective viruses considering discrete dynamics were early studied,  
69 and the presence of deterministic chaos was suggested [18]. Later, detailed mathematical  
70 models of serial passage predicted irregular fluctuations in virus titer, claimed to be also  
71 representative of deterministic chaos [19,20]. Although these studies suggested the  
72 presence of chaos, the confirmation of chaotic dynamics in theoretical models of helper and  
73 DI viruses was not thoroughly provided. All these observations suggest that the interactions  
74 between helper and DI viruses may in some cases lead to more complex interactions than  
75 those postulated by the ‘Von Magnus’ model.

76 For baculoviruses regular cyclical changes in virus titer have not been observed during  
77 passages in insect cells (e.g., [5]), although De Gooijer *et al.* [21] observed patterns likely

78 caused by the presence of DI viruses in bioreactors [22,23]. Moreover, few studies have  
79 tracked DI baculovirus levels over time [6,24]. In this study, we therefore first sought to  
80 observe experimentally and better understand the dynamics of DI baculoviruses. We  
81 employed quantitative real-time PCR (qPCR) to consider how levels of helper and DI  
82 baculoviruses change over a high number of passages in insect cells. Given that we  
83 observed irregular fluctuations in the titers of both helper and DI viruses, we then explored  
84 the characteristics of a simple mechanistic mathematical model that produced patterns  
85 qualitatively similar to the data. Our experimental observations and theoretical results help  
86 shed light on the question of whether the dynamics of virus populations harboring DIs are  
87 chaotic.

88

## 89 **2 Methods**

90

### 91 **2.1 Serial passage in insect cells**

92

93 For our experiments, bGFP was serially passaged in insect cells. bGFP is a bacmid-derived  
94 [25] alphabaculovirus, *Autographa californica multiple nucleopolyhedrovirus* (AcMNPV),  
95 expressing GFP under the polyhedrin promoter [5]. One hundred minimal-dilution (e.g., 1:4  
96 dilution) serial passages were performed in a monolayer of approximately  $10^6$  Sf21 cells [26]  
97 in 25 ml flasks [5]. For the first passage, 20 median tissue culture infectious dose units per  
98 cell were added. The cells were exposed to the virus for 2 h, followed by the refreshing of  
99 media and incubation of the cells for 72 h. The media collected at the end of a passage was  
100 used for passaging and as samples for analysis.

101

### 102 **2.2 qPCR**

103

104 We quantified the concentration of the *ie1* and *p94* genes in budded virus samples from the  
105 serially passaged baculovirus with a SYBR Green I based qPCR assay [24]. DNA was  
106 extracted from stored media and analyzed by qPCR as described elsewhere [27]. For *ie1*,  
107 the forward primer 5'- TCGGAATCCCTTGAGCAGCCTG-3' and reverse primer 5'-  
108 TTGCCGATGGTTGGTTCACACC-3' were used. For *p94*, the forward primer 5'-  
109 CCGAGACATACCACAAAGCCG-3' and reverse primer 5'-  
110 GCACATAAACGACGCAGAATACAT-3' were used. As an internal control, samples were  
111 spiked with  $10^9$  copies of a plasmid containing luciferase prior to DNA extraction (pGEM-luc;  
112 Promega). The forward primer 5'-TGTTGGGCGCGTTATTTATC- 3' and reverse primer 5'-  
113 AGGCTGCGAAATGTTTCATACT-3' were used to amplify luciferase, as previously described  
114 [28]. DNA concentrations for all three templates were calculated from fluorescence levels  
115 using comparative analysis in RotorGene 6.0 Software (Corbett Research; Sydney,  
116 Australia). The *ie1* and *p94* levels were divided by measured luciferase DNA concentration  
117 for normalization. Five time points could not be analyzed for various technical reasons (i.e.,  
118 sample volume available, low yields of DNA upon extraction).

119 Statistical analyses were performed with the statistical software package R version  
120 2.14.2 (The R Foundation; Vienna, Austria) or SPSS 20.0 (IBM Corporation, Armonk, NY,  
121 USA).

122

### 123 **2.3 Simple probabilistic model of DI dynamics**

124

125 In order to model infection dynamics for our system, we assume that during infection of  
126 insect cells each virion acts independently, and that the dynamics of infection during serial  
127 passaging can be captured by only considering the first round of cellular infection during  
128 each passage. Moreover, for simplicity we assume that each virion produced will infect a cell  
129 in the next round of passaging. We can make this assumption because we are considering  
130 processes within the cell (i.e., replication), and we do not have to consider both virion

131 numbers produced and probabilities of infection in any detail. As virions act independently,  
 132 the number of infecting virions per cell follows a Poisson distribution for each virus. These  
 133 distributions will have means  $\psi_H = n_H/c$  for the helper virus and  $\psi_D = n_D/c$  for the DI virus,  
 134 where  $n_H$  is the number of helper virions,  $n_D$  is the number of DI virions and  $c$  is the number  
 135 of cells. We then consider the frequency of cells infected only by the helper virus,  $\alpha$ , or co-  
 136 infected by both viruses,  $\beta$ , since of all cells there will only be virus production in these two  
 137 fractions. Following [28], the infection probabilities are given by:

$$138 \quad \alpha = \Pr(H \cap \bar{D}) = e^{-\psi_D}(1 - e^{-\psi_H}), \quad (1)$$

$$139 \quad \beta = \Pr(H \cap D) = (1 - e^{-\psi_D})(1 - e^{-\psi_H}), \quad (2)$$

140 where  $\Pr(H \cap \bar{D})$  is the probability a cells will be infected by the helper virions but not by DI  
 141 virions, and  $\Pr(H \cap D)$  is the probability a cell will be infected by both helper and DI virions.  
 142 Those cells infected by only the helper virus produce  $v_\alpha$  virions per cell. However, the helper  
 143 virus mutates into a DI with a probability  $\mu$ . In co-infected cells, mainly DIs are produced at a  
 144 rate of  $v_\beta$  virions per cell. However, we allow for the possibility that production of virions in  
 145 co-infected cells is leaky, allowing a proportion  $\phi$  of virions to be of the helper virus type.  
 146 Hence the production of helper and DI virions during a passage,  $t$ , is:

$$147 \quad n_H(t + 1) = c(\alpha v_\alpha(1 - \mu) + \beta v_\beta \phi), \quad (3)$$

$$148 \quad n_D(t + 1) = c(\alpha v_\alpha \mu + \beta v_\beta(1 - \phi)). \quad (4)$$

149 There are a number of other sources of variation during serial passage experiments  
 150 besides the distribution of helper and DI viruses over cells. Mutation from helper virus to DI  
 151 virus is an inherently stochastic process and is therefore an unavoidable source of variation  
 152 in experiments. We assume these mutations occur in those cells infected only by the helper  
 153 virus ( $c_H = \alpha c$ ), and that the number of cells in which a mutation occurs follows a binomial  
 154 distribution with a probability of success  $\chi$  :

$$155 \quad \Pr(\Omega = \omega) = \binom{c_H}{\omega} \chi^\omega (1 - \chi)^{c_H - \omega}, \quad (5)$$



156 where  $\Omega$  is a random variable describing the number of cells in which a mutation occurs, and  
157  $\omega$  is a realization of  $\Omega$ . For each passage, one realization of this binomial process  $\omega$  can  
158 then be divided by  $c_H$  and substituted for  $\mu$  in (3) and (4). This addition renders a model  
159 incorporating the minimal conceivable stochastic variation due to mutations of helper virus to  
160 DI virus.

161 Stauffer Thompson and Yin [17] considered the effects of various sources of  
162 experimental error on the dynamics of helper and DI virus, and concluded the most important  
163 source of variation was the number of available cells. To consider what effects plausible  
164 sources of variation – other than mutation of helper virus to a DI virus – might have on the  
165 dynamics of virus population harboring DI viruses, we therefore allow the number of cells to  
166 follow a negative binomial distribution, such that:

$$167 \quad \Pr(X = x) = \frac{\Gamma(x+r)}{\Gamma(r)x!} p^r (1-p)^x, \quad (6)$$

168 where  $X$  is a random variable describing the number of cells used in each passage,  $x$  is a  
169 realization of  $X$  and for each passage one realization is valid,  $p$  is the probability of success  
170 for a trial,  $r$  is the number of successful trials required and  $\Gamma()$  is the gamma function. The  
171 negative binomial distribution was chosen because it is a discrete probability distribution for  
172 which we can change the variance without changing the mean [29], and can therefore  
173 consider variances higher than those of a Poisson distribution. Note that we attach no  
174 significance to particular  $p$  and  $r$  values or their interpretation here, these were chosen simply  
175 to increase the variance of the distribution of the number of cells to levels likely to be seen in  
176 experiments, while keeping the mean constant.

177 Finally, DI baculoviruses are known to accumulate multiple copies of particular loci,  
178 such as the non-HR origin of DNA replication in the *p94* gene [8-10]. If the detection of DIs is  
179 sequence-based, the observed DI virus level,  $n'_D(t)$ , could diverge from the actual number of  
180 virions,  $n_D(t)$ , increasing over passages because multiple copies of the specific sequence  
181 used for detection accrue in DI genomes. If the interactions between helper and DI viruses

182 remain otherwise identical, the observed DI virus level at passage  $t$  will be:

$$183 \quad n'_D(t) = (1 + t\xi)n_D(t), \quad (7)$$

184 where  $\xi$  is the rate of change in the mean number of DI detection sequences per DI genome  
185 per passage. The model was implemented with the statistical software package R 2.14.2.

186

## 187 **2.4 Computation of the maximal Lyapunov exponent**

188

189 Here we describe the procedure to compute the maximal Lyapunov exponent (hereafter  
190 MLE) for a discrete dynamical system [30,31] that will be used for our mathematical model.

191 The characteristic Lyapunov exponents are usually introduced to measure the rate of  
192 exponential divergence of nearby trajectories in the phase space, i.e., they give us  
193 information on the rate of growth of a very small error on the initial state of the system [32-  
194 34]. We consider the discrete dynamical system of the following form:

$$195 \quad x_{i+1} = F_i(x_i), \quad i = 0, 1, \dots \quad (8)$$

196 with a given  $x_0$ ,  $x_i \in \mathbb{R}^n$  and  $F_i$  being assumed to be continuously differentiable. Small  
197 perturbations to the orbits  $\{x_i\}$  of (8) evolve according to the dynamics of the respective  
198 linear variational equations:

$$199 \quad Y_{i+1} = DF_i(x_i)Y_i = A_i Y_i, \quad i = 0, 1, \dots$$

200 with  $Y_i \in \mathbb{R}^{n \times n}$  and  $Y_0 = I$ . The matrix  $A_i = \left( \frac{\partial F_i(x)}{\partial x} \right) \Big|_{x=x_i} \in \mathbb{R}^{n \times n}$  is assumed to be full rank

201 in order to obtain the  $n$  Lyapunov exponents. Let  $Y_0 = I$  and  $Y_i = A_{i-1} \dots A_0$ ;  $i = 0, 1, \dots$ , be  
202 the fundamental solution of (8). Then the following symmetric positive definite matrices exist:

$$203 \quad \Delta = \lim_{t \rightarrow \infty} [(Y_t)^T Y_t]^{1/(2t)}.$$

204 The logarithms of their eigenvalues are called Lyapunov exponents of (8), and are denoted  
205 as  $\lambda_1 > \lambda_2 > \dots > \lambda_n$ ; with  $\lambda_1$  being the MLE.

206 We emphasize that Lyapunov exponents give us information on the typical behavior  
207 along a generic trajectory, followed for infinite time and keeping the initial perturbation

208 infinitesimally small. The rate of separation can be different for different orientations of the  
209 initial separation vector. Therefore, there is a spectrum of Lyapunov exponents – which is  
210 equal to the dimensionality of the phase space,  $\lambda_1 > \lambda_2 > \dots > \lambda_n$ . A positive MLE is  
211 commonly taken as an indicator of chaotic behavior (provided some conditions are met, e. g.,  
212 phase space compactness).

213

### 214 **3 Results and Discussion**

215

#### 216 **3.1 qPCR-determined *ie1* and *p94* levels indicate complex dynamics**

217

218 The AcMNPV-derived bGFP was passaged for 100 passages in Sf21 cells, and we then  
219 determined the level of the *ie1* and *p94* genes by qPCR for the ancestral virus and passages  
220 50-100 (Figure 1). The analysis focused on a virus population with a high number of  
221 passages, as we wanted to focus on the dynamics of a population containing DIs rather than  
222 their *de novo* generation, which has already been documented [5,6,24,35]. The  
223 concentration of *ie1* was used as a proxy for helper virus titers, because this gene encodes  
224 an essential transcriptional regulator [36]. All viruses capable of autonomous replication  
225 must therefore carry *ie1*. As a proxy for DI virus titers, we used the concentration of *p94* –  
226 *ie1*, which we subsequently refer to as *p94\**. This value gives an approximation of DI levels  
227 because *p94* contains a non-HR origin of DNA replication that is maintained and selected for  
228 in DI viruses [8-10,24], and by subtracting *ie1* we consider only the concentration of those  
229 viruses missing this essential gene. However, not all DI viruses need necessarily contain  
230 *p94*, and some DI viruses could in principle contain *ie1*. Our measurement is therefore a  
231 proxy, although previous results suggest it is a good indicator of the frequency of DI viruses  
232 [24]. qPCR-measured *ie1* levels were significantly lower than both *p94* and *p94\** levels  
233 (Wilcoxon signed ranks test:  $z = -5.905$ ,  $P < 0.001$ ), in agreement with previous observations

234 [24].

235 *Prima facie* there appear to be no regular oscillations in *ie1* and *p94\** levels. Our  
236 results therefore contrast with previous findings for other viruses, where helper and DI  
237 viruses changed titers out of phase [14,16] and with evident regular periodicity [14]. There  
238 appears to be an increase over passages of *p94\** levels, whereas *ie1* levels, although also  
239 showing a great deal of variation, appear to be stationary (Figure 1). To test if this is indeed  
240 the case, we performed a non-parametric Spearman test to look for correlations between *ie1*  
241 or *p94\** levels and time. There was no significant trend for *ie1* ( $\rho = 0.277$ , 44 d.f.,  $P = 0.062$ ),  
242 suggesting that minimum helper virus frequencies had already been reached by passage 50.  
243 On the other hand, *p94\** increased significantly over passages ( $\rho = 0.654$ , 44 d.f.,  $P < 0.001$ ),  
244 suggesting that DI genomes accumulated multiple copies of the non-HR origin of DNA  
245 replication in their genomes [8-10]. This trend could, however, also result from an overall  
246 increase in the number of DI viruses present per helper virus, indicating the DI virus is  
247 optimizing its exploitation of the helper virus.

248 The levels of *ie1* and *p94\** varied greatly between passages, and the two levels of  
249 viruses appear to change in phase (Figure 1). A Model II major-axis linear regression [37] on  
250 log-transformed *ie1* and *p94\** concentrations rendered a slope significantly greater than zero  
251 (0.965 with a 95% confidence interval 0.713-1.301;  $P < 0.001$ ), confirming a relationship  
252 between the two variables (Figure 2). This relationship in turn is congruent with the  
253 observation that the two viruses change levels in phase: when the level of DI virus is high,  
254 the level of helper virus also tends to be high and vice-versa.

255

### 256 **3.2 Simple models of DI dynamics**

257

258 Measurements of *ie1* and *p94\** levels by qPCR gave surprising results, as the helper and DI  
259 viruses changed levels in phase and the length of oscillations appeared to be irregular. To

260 better understand these results, we built a simple probabilistic model describing the  
261 interactions between helper and DI virus infecting insect cells. The model incorporates  
262 stochasticity in the number of cells in which helper viruses will mutate to DI viruses (see  
263 Methods section “Simple probabilistic model of DI dynamics”).

264 For some parameter sets, the model leads to an equilibrium state or oscillatory  
265 dynamics. Moreover, our model can also generate more complex behavior like quasi-  
266 periodic or chaotic dynamics (Figures 3 and 4). This behavior is more similar – in a  
267 qualitative sense – to our empirical observations (Figure 1). In these cases, the oscillatory  
268 dynamics are not completely regular and the two viruses can oscillate at different levels (i.e.,  
269  $n_D \gg n_H$ ). For instance, the dynamics represented in the  $(n_H, n_D)$  phase space shows a ring-  
270 like attractor formed by a broad cloud of points due to stochasticity (Figure 3c). In order for  
271 the model to generate behavior qualitatively similar to the data, we required values for the  
272 number of insect cells ( $c$ ) one order of magnitude smaller than the estimated number of cells  
273 used in serial passage experiments. As  $c_H$  depends on  $c$ , stochastic effects will become  
274 stronger as the number of cells decrease [see (5)]. Hence, this disparity suggests that there  
275 are other sources of variation in our experiment, or alternatively that a small number of  
276 infected cells actually contribute to the viable virus progeny being passaged.

277

### 278 **3.3 Chaos in the dynamics of helper and DI viruses**

279

280 The time series in Figure 3 and the attractor in Figure 3d suggest the presence of complex  
281 dynamics. In order to investigate the possible array of dynamical behaviors arising from our  
282 model, we built bifurcation diagrams using mutation rate as control parameter, and identified  
283 several parameter regions suggesting chaotic behavior. The bifurcation diagram was first  
284 built considering a large population of insect cells to minimize stochastic effects (Figure 3e).  
285 Moreover, similar results were obtained for our model when the rate of mutation ( $\mu$ ) was fixed  
286 (Figure 4a). Therefore, when we remove the stochastic component, our simple probabilistic

287 model appears to exhibit deterministic chaos, in agreement with previous theoretical studies  
288 suggesting this type of dynamics among helper and DI viruses [18,20].

289 In order to properly identify the presence of chaos in our model we computed the MLE  
290 (see section 2.4). The Lyapunov exponents are used as a convenient indicator of the  
291 exponential divergence of close initial conditions, which is characteristic of chaotic dynamics  
292 [38,39]. The results of the MLE computation are shown in Figure 4. We first show the same  
293 bifurcation diagram previously computed (Figure 3e), but now removing stochasticity (i.e., a  
294 variable rate of mutation). The dynamics clearly show a pattern of a series of bifurcations at  
295 decreasing mutation rate. Below the bifurcation diagram we show the MLE computed for the  
296 same range of mutation rates used in the bifurcation diagram (Figure 4b). We notice that the  
297 MLE allows us to identify two interesting dynamical properties: (i) chaos and (ii) bifurcations.  
298 In this sense, chaotic dynamics arises when the MLE is positive. For example, see the  
299 chaotic window in the parameter range  $0.5 \lesssim \mu \lesssim 0.57$ . On the other hand, bifurcations  
300 occur when the MLE is zero. At decreasing mutation there is a first bifurcation occurring  
301 when  $\mu \approx 0.9$ , and then there are a series of flip bifurcations that involve oscillatory (i.e.,  
302 periodic and quasi-periodic), but not chaotic, dynamics within the range  $0.7 \lesssim \mu \lesssim 0.8$ . Such  
303 a series of flip bifurcations suggest the presence of a Ruelle-Takens-Newhouse (or  
304 quasiperiodic) route to chaos [38]. The Ruelle-Takens-Newhouse transition to chaos  
305 involves that as the control parameter (mutation rate in our system) is changed, the  
306 dynamics undergoes a series of flip bifurcations giving place to periodic and toroidal or  
307 quasiperiodic attractors that then become unstabilized giving place to a strange attractor (i.e.,  
308 with positive Lyapunov exponents), as we show in Figure 4. A further decrease of mutation  
309 can cause chaotic dynamics (see positive values of the MLE in Figure 4b). Previous  
310 theoretical studies have suggested that DI virus dynamics could exhibit deterministic chaos  
311 [18,20]. However, these studies did not provide dynamical measures (e.g., Lyapunov  
312 exponents) confirming the presence of chaos. Finally, we notice that chaotic windows using

313  $\mu$  as control parameter and tuning other model parameters were also found (results not  
314 shown).

315

### 316 **3.4 Predicted effects of experimental variation on dynamics of helper and DI viruses**

317

318 The analysis of MLE was performed on a deterministic model, which does not include the  
319 effects of experimental variation. Although this analysis suggests the presence of  
320 deterministic chaos in the simple model presented (Figure 4), the apparently irregular and  
321 possibly chaotic patterns in the actual experimental data could conceivably arise because of  
322 experimental variation. To assess what the impact of experimental variation may be, we  
323 included an important source of experimental variation in our model: variation in the number  
324 of cells over passages [17]. Using the same model parameters as in Figure 3, we  
325 considered two  $\mu$  values: (i) 0.35, for which the MLE is  $-0.068$ , and (ii) 0.74, for which the  
326 MLE is  $-0.005$ . These values were chosen to consider situations in which the deterministic  
327 model clearly predicts non-chaotic dynamics ( $\mu = 0.35$ ), and a situation in which the MLE  
328 approaches positive values ( $\mu = 0.74$ ). We then ran simulations of the deterministic model  
329 (Figure 5a and 5b) and simulations incorporating variability in the number of cells (Figure 5c  
330 and 5d; see Methods section for details), and stochasticity in the occurrence of mutations  
331 (Figure 5e and 5f). These simulations show that, for parameter values that the deterministic  
332 model predicts non-chaotic dynamics, stochasticity in mutation and variation in the number of  
333 cells can both generate time series with irregular fluctuations similar to our experimental  
334 observations. However, for the given parameter values the effects of mutation were stronger  
335 than the effects of variation in the number of cells.

336 These results suggest that our analysis of the deterministic model needs to be  
337 interpreted cautiously. A simple deterministic model inspired by experimental data displays  
338 chaotic dynamics, but even for parameter values for which the model dynamics are not  
339 predicted to be chaotic, irregular patterns similar to the data can be observed if sources of

340 variation are included in the model. Moreover, the stochasticity induced by mutation is  
341 inherent to the system. In other words, even if a perfect experiment was conducted (there  
342 would be no experimental variation whatsoever; i.e., cell number was held constant over  
343 passages), mutation would still be a source of stochasticity. We cannot, therefore,  
344 unequivocally attribute irregular changes in virus titer over passages to purely deterministic  
345 chaotic dynamics. What we can conservatively conclude is that even a simple deterministic  
346 model, one that excludes a source of stochasticity inherent to the experimental system,  
347 generates chaotic dynamics. Although we cannot exclude that stochastic processes are also  
348 responsible for the surprising experimental observations, our work helps bolster the case that  
349 deterministic chaos is a plausible hypothesis. Moreover, the consideration of stochasticity is  
350 not incompatible with the result that standard-DIs dynamics may behave chaotically, leading  
351 to complex fluctuation patterns (see section 4).

352

#### 353 **4 Conclusions**

354

355 By monitoring the dynamics of helper and DI baculovirus levels over passages in insect cells  
356 we observed that the titers of both viruses oscillated irregularly, suggesting the presence of  
357 chaos. A simple stochastic model of DI dynamics illustrated how such irregular cyclical  
358 dynamics could be generated, a result similar to that obtained by others [17,18,20]. Early  
359 theoretical studies on helper and DI viruses predicted oscillations [18], and even suggested  
360 the possibility of chaotic attractors governing the dynamics of these types of systems [18,20].  
361 Our results demonstrate that the ‘Von Magnus’ model may be too simple to explain the  
362 dynamics of DI baculoviruses in insect cells. The observed dynamics hint that the evolution  
363 of virus levels over time may very well be chaotic, as suggested by Szathmary [18] and  
364 Kirkwood and Bangham [20].

365 Our simple model without stochasticity generated chaos, and both bifurcation diagrams



366 and Lyapunov exponents analyses revealed a quasiperiodic (i.e., Ruelle-Takens-Newhouse)  
367 route to chaos at decreasing mutation rates generating defective particles. Although  
368 previous studies [18,20] suggested the presence of chaos underlying the dynamics of helper  
369 and DI viruses, these authors did not provide quantitative measures of chaos. By computing  
370 the MLE we have numerically shown that for some parameter regions chaos is found in this  
371 type of system. Such a finding has important implications for the predictability of DI  
372 dynamics in insect cells, making it impossible to accurately predict dynamics in the long term  
373 even if the composition of a virus population (i.e., initial condition) is known. On the other  
374 hand, we cannot discard the notion that experimental variation – especially stochasticity in  
375 the helper virus mutating to a DI virus – may play an important role in generating the  
376 dynamical patterns we have observed. However, noise may not be incompatible with chaotic  
377 behavior: it has been suggested that a system with negative Lyapunov exponent in the  
378 absence of noise can have a positive stochastic Lyapunov exponent when noise is  
379 introduced [40]. In this sense, possible sources of noise in our experiments such as  
380 stochastic mutation or variation in the number of insect cells could increase parameter  
381 regions displaying chaos (see Figs. 3e and 5). Previous studies of the geometry of the  
382 attractors found in the driven anharmonic oscillator revealed that increased noise levels  
383 could induce a transition to chaotic behavior [41]. Hence, rather than destabilizing or  
384 eradicating chaotic motions in the phase space, noise can enhance chaos, while destroying  
385 periodic orbits. Actually, local instabilities responsible for the deterministic chaos actually  
386 increased the observability of chaos in the presence of fluctuations [41,42].

387 We have presented a simple model of DI dynamics in order to better elucidate the  
388 mechanisms underlying the experimentally observed behavior. The use of simple  
389 mathematical models makes it easier to identify mechanisms underlying different dynamics.  
390 On the other hand, we could only consider whether particular qualitative aspects of model  
391 behavior were supported by the data. Furthermore, it was recently shown that  
392 alphabaculovirus populations passaged in insect cells accumulate multiple DI viruses [6], a

393 conclusion supported by the different qPCR-measured levels for 4 different loci in passaged  
394 baculovirus populations [24]. Here we only modeled one helper virus and one DI virus, a  
395 reasonable approach given that our qPCR-based proxies, *ie1* and *p94\** levels, are also  
396 dichotomous.

397

## 398 **5 Acknowledgements**

399

400 The authors thank Javier Carrera, Just Vlak and Lia Hemerik for helpful discussion. MPZ  
401 was supported by a Rubicon Grant from the Netherlands Organization for Scientific  
402 Research (NWO, [www.nwo.nl](http://www.nwo.nl)) and a 'Juan de la Cierva' postdoctoral contract (JCI-2011-  
403 10379) from the Spanish 'Secretaría de Estado de Investigación, Desarrollo e Innovación'.  
404 JS was supported by the Botín Foundation. SFE was supported by grant BFU2012-30805,  
405 also from the Spanish 'Secretaría de Estado de Investigación, Desarrollo e Innovación'.

406

## 407 **References**

408

- 409 1. Von Magnus, P.: Incomplete forms of influenza virus. *Adv. Virus. Res.* **2**, 59-79  
410 (1954)
- 411 2. Huang, AS.: Defective interfering viruses. *Annu. Rev. Microbiol.* **27**, 101-117 (1973)
- 412 3. Kool, M., Voncken, J.W., Vanlier, F.L.J., Tramper, J., Vlak, J.M.: Detection and  
413 analysis of *Autographa californica* nuclear polyhedrosis-virus mutants with defective  
414 interfering properties. *Virology* 183, 739-746 (1991)
- 415 4. Wickham, T.J., Davis, T., Granados, R.R., Hammer, D.A., Shuler, M.L., Wood, H.A.:  
416 Baculovirus defective interfering particles are responsible for variations in  
417 recombinant protein-production as a function of multiplicity of infection. *Biotechnol.*  
418 *Lett.* **13**, 483-488 (1991)

- 419 5. Pijlman, G.P., van den Born, E., Martens, D.E., Vlak, J.M.: *Autographa californica*  
420 baculoviruses with large genomic deletions are rapidly generated in infected insect  
421 cells. *Virology* **283**, 132-138 (2001)
- 422 6. Giri, L., Feiss, M.G., Bonning, B.C., Murhammer, D.W.: Production of baculovirus  
423 defective interfering particles during serial passage is delayed by removing  
424 transposon target sites in fp25k. *J. Gen. Virol.* **93**, 389-399 (2012)
- 425 7. King, L.A., Possee, R.D.: *The Baculovirus Expression System*. University Press,  
426 Cambridge (1992)
- 427 8. Lee, H.Y., Krell, P.J.: Reiterated DNA fragments in defective genomes of *Autographa*  
428 *californica* nuclear polyhedrosis virus are competent for AcMNPV-dependent DNA  
429 replication. *Virology* **202**, 418-429 (1994)
- 430 9. Pijlman, G.P., Dortmans, J., Vermeesch, A.M.G., Yang, K., Martens, D.E., Goldbach,  
431 R.W., Vlak, J.M.: Pivotal role of the non-hr origin of DNA replication in the genesis of  
432 defective interfering baculoviruses. *J. Virol.* **76**, 5605-5611 (2002)
- 433 10. Pijlman, G.P., van Schijndel, J.E., Vlak, J.M.: Spontaneous excision of BAC vector  
434 sequences from bacmid-derived baculovirus expression vectors upon passage in  
435 insect cells. *J. Gen. Virol.* **84**, 2669-2678 (2003)
- 436 11. Pijlman, G.P., Vermeesch, A.M.G., Vlak, J.M.: Cell line-specific accumulation of the  
437 baculovirus non-hr origin of DNA replication in infected insect cells. *J. Invertebr.*  
438 *Pathol.* **84**, 214-219 (2003)
- 439 12. Roux, L., Simon, A.E., Holland, J.J.: Effects of defective interfering viruses on virus-  
440 replication and pathogenesis *in vitro* and *in vivo*. *Adv. Virus. Res.* **40**, 181-211 (1991)
- 441 13. Grabau, E.A., Holland, J.J.: Analysis of viral and defective-interfering nucleocapsids  
442 in acute and persistent infection by Rhabdoviruses. *J. Gen. Virol.* **60**, 87-97 (1982)
- 443 14. Kawai, A., Matsumoto, S., Tanabe, K.: Characterization of Rabies viruses recovered  
444 from persistently infected BHK cells. *Virology* **67**, 520-533 (1975)
- 445 15. Roux, L., Holland, J.J.: Viral genome synthesis in BHK-21 cells persistently infected

- 446 with Sendai virus. *Virology* **100**, 53-64 (1980)
- 447 16. Palma, E.L., Huang, A.: Cyclic production of vesicular stomatitis virus cause by  
448 defective interfering particles. *J. Infect. Dis.* **129**, 402-410 (1974).
- 449 17. Stauffer Thompson, K.A., Yin, J.: Population dynamics of an RNA virus and its  
450 defective interfering particles in passage cultures. *Virol. J.* **7**, 257-266 (2010)
- 451 18. Szathmáry, E.: Cooperation and defection – playing the field in virus dynamics. *J.*  
452 *Theor. Biol.* **165**, 341-356 (1993)
- 453 19. Bangham, C.R.M., Kirkwood, T.B.L.: Defective interfering particles – effects in  
454 modulating virus growth and persistence. *Virology* **179**, 821-826 (1990)
- 455 20. Kirkwood, T.B.L., Bangham, C.R.M.: Cycles, chaos, and evolution in virus cultures –  
456 a model of defective interfering particles. *Proc. Natl. Acad. Sci. USA* **91**, 8685-8689  
457 (1994)
- 458 21. De Gooijer, C.D., Koken, R.H.M., van Lier, F.L.J., Kool, M., Vlak, J.M., Tramper, J.: A  
459 structured dynamic model for the baculovirus infection process in insect-cell reactor  
460 configurations. *Biotech. Bioeng.* **40**, 537-548 (1992)
- 461 22. Van Lier, F.L.J., van der Meijs, W.C.J., Grobber, N.G., Olie, R.A., Vlak, J.M.,  
462 Tramper, J.: Continuous beta-galactosidase production with a recombinant  
463 baculovirus insect-cell system in bioreactors. *J. Biotechnol.* **22**, 291-298 (1992)
- 464 23. Van Lier, F.L.J., van den Hombergh, J., de Gooijer, C.D., den Boer, M.M., Vlak, J.M.,  
465 Tramper, J.: Long-term semi-continuous production of recombinant baculovirus  
466 protein in a repeated (fed-)batch two-stage reactor system. *Enzyme Microb. Technol.*  
467 **18**, 460-466 (1996)
- 468 24. Zwart, M.P., Erro, E., van Oers, M.M., de Visser, J.A.G.M., Vlak, J.M.: Low multiplicity  
469 of infection in vivo results in purifying selection against baculovirus deletion mutants.  
470 *J. Gen. Virol.* **89**, 1220-1224 (2008)
- 471 25. Luckow, V.A., Lee, S.C., Barry, G.F., Olins, P.O.: Efficient generation of infectious  
472 recombinant baculoviruses by site-specific transposon-mediated insertion of foreign

- 473 genes into a baculovirus genome propagated in *Escherichia coli*. J. Virol. **67**, 4566-  
474 4579 (1993)
- 475 26. Vaughn, J.L., Goodwin, R.H., Tompkins, G.J., McCawley, P.: Establishment of 2 cell  
476 lines from insect *Spodoptera frugiperda* (Lepidoptera, Noctuidae). In Vitro **13**, 213-  
477 217 (1977)
- 478 27. Zwart, M.P., van Oers, M.M., Cory, J.S., van Lent, J.W.M., van der Werf, W., Vlak,  
479 J.M.: Development of a quantitative real-time PCR for determination of genotype  
480 frequencies for studies in baculovirus population biology. J. Virol. Meth. **148**, 146-154  
481 (2008).
- 482 28. Zwart, M.P., Hemerik, L., Cory, J.S., de Visser, J.A.G.M., Bianchi, F.J.J.A., van Oers,  
483 M.M., Vlak, J.M., Hoekstra, R.F., van der Werf, W.: An experimental test of the  
484 independent action hypothesis in virus-insect pathosystems. Proc. R. Soc. B **276**,  
485 2233-2242 (2009)
- 486 29. Olkin, I., Gleser, L.J., Derman, C.: Probability Models and Applications. Macmillan,  
487 New York (1994)
- 488 30. Parker, T., Chua, L.: Practical Numerical Algorithms for Chaotic Systems Springer-  
489 Verlag, Berlin (1989)
- 490 31. Dieci, L., van Vleck, E.S.: Computation of a few Lyapunov exponents for continuous  
491 and discrete dynamical systems. J. Appl. Num. Math. **17**, 275-291 (1995)
- 492 32. Matsumoto, T., Chua, L.O., Komuro, M.: The double scroll. IEEE Trans. Circuits Syst.  
493 **32**, 797-818 (1985)
- 494 33. Chua, L.O., Komuro, M., Matsumoto, T.: The double scroll family: Rigorous proof of  
495 chaos. IEEE Trans. Circuits Syst. **33**, 1072-1097 (1986)
- 496 34. Ramasubramanian, K., Sriram, M.S.: A comparative study of computation of  
497 Lyapunov spectra with different algorithms. Physica D: Nonlin. Phenom. **139**, 72-86  
498 (2000)

- 499 35. Lee, H.Y., Krell, P.J.: Generation and analysis of defective genomes of *Autographa*  
500 *californica* nuclear polyhedrosis virus. J. Virol. **66**, 4339-4347 (1992)
- 501 36. Kovacs, G.R., Choi, J., Guarino, L.A., Summers MD: Functional dissection of the  
502 *Autographa californica* nuclear polyhedrosis virus Immediate Early 1 transcriptional  
503 regulatory protein. J. Virol. **66**, 7429-7437 (1992)
- 504 37. Legendre, P., Legendre, L., Numerical Ecology. Elsevier, Amsterdam (1998)
- 505 38. Schuster, H.G.: Deterministic chaos: An introduction. Wiley-VCH Verlag GmbH & Co.  
506 KGaA, Weinheim (2005)
- 507 39. Strogatz, S.H.: Nonlinear Dynamics and Chaos: With Applications to Physics,  
508 Biology, Chemistry and Engineering: Westview Press, Cambridge (1994)
- 509 40. Dennis, B., Desharnais, R.A., Cushing, J.M., Henson, S.M., Constantino, R.F.: Can  
510 noise induce chaos? Oikos **102**, 329-339 (2003)
- 511 41. Crutchfield, J.P., Huberman, B.A.: Fluctuations and the onset of chaos. Phys. Lett. A  
512 **77**, 407-410 (1980)
- 513 42. Crutchfield, J.P., Farmer, J.D.: Fluctuations and simple chaotic dynamics. Phys. Rep.  
514 **92**, 45-82 (1982)
- 515

516 **Figure Legends**

517

518 **Figure 1.** Experimental data with the passage number given on the abscissae, and the log  
519 concentration of *ie1* (open triangles) and *p94\** (filled squares) given on the ordinate (error  
520 bars represent the standard error). Consecutive data points are connected by solid lines,  
521 whereas a dotted line is used when there are missing data. *ie1* is used as a proxy for helper  
522 virus concentration, and *p94\** as a proxy for DI virus concentration. The concentration of  
523 *p94\** is much higher than *ie1* for all passages. There are large changes in concentration of  
524 both loci over passages, *p94\** concentration increases significantly over passages. Note that  
525 the two loci appear to generally change concentration in phase. qPCR was also performed  
526 on the ancestral virus rendering similar log concentrations of  $6.582 \pm 0.044$  for *ie1* and  
527  $6.587 \pm 0.038$  for *p94*, the unadjusted level of the *p94* gene. The ancestral population  
528 therefore has a 1:1 ratio of the two templates, indicating DI viruses are not present.

529

530 **Figure 2.** Model II major-axis regression on the log *ie1* titer (abscissae) vs. log *p94\** levels  
531 (ordinate).

532

533 **Figure 3.** Dynamical behavior of the DI mathematical model. Panel (a) and (b) are time  
534 series generated by the model, with the black lines representing the level of the helper virus  
535 and the red line the observed level of the DI virus ( $n'_D$ ). The model can generate a  
536 combination of irregular oscillations, much higher levels of DI ( $n'_D$ ) than helper virus ( $n_H$ ), and  
537 virus levels which change almost in phase (in the periodic and chaotic behaviors). In all plots  
538 we used  $v_\alpha = 10$ ,  $v_\beta = 25$  and  $\phi = 0.0002$ . For panels (a-d)  $\xi = 0.01$ , whereas  $\xi = 0$  for Panel  
539 (e). In (a)  $c = 10^4$  and  $\mu = 0.78$ , and in (b)  $c = 5 \times 10^5$  and  $\mu = 0.61$ . Panel (c) shows a noisy,  
540 ring-like attractor in the phase space obtained by plotting the population numbers of the  
541 helper virus on the x-axis and the DI virus on the y-axis for  $c = 10^5$  and  $\mu = 0.78$ . Panel (e) is

542 a bifurcation diagram, for which the model was run for 300 serial passages. We increased  $\mu$   
543 (the mutation rate) from 0 to 1 by increments of  $1 \times 10^{-3}$  (abscissae), and then plotted the  
544  $\log_{10}$ -transformed DI virus levels ( $n_D$ ) over the last 100 passages (ordinate). The model was  
545 run with a large number of cells ( $c = 10^7$ ) to minimize stochasticity and no differences in  
546 observed DI numbers [ $\xi = 0$  in (7)] so that virus levels could be compared over passages  
547 (i.e.,  $n_D = n'_D$ ). The results suggest a series of bifurcations although there is some variation in  
548 the dynamics for all  $\mu$  values due to the stochasticity of the model. We therefore performed  
549 the same analysis without stochastic effects (the mutation rate for each passage is  $\mu$ , and not  
550 a realization of  $\Omega$ ), which makes it possible to observe clearly the structure of the chaotic  
551 attractor using  $c = 10^7$  and  $\mu = 0.61$  (Panel d). We also generated a bifurcation diagram  
552 without stochastic effects (Figure 4a).

553

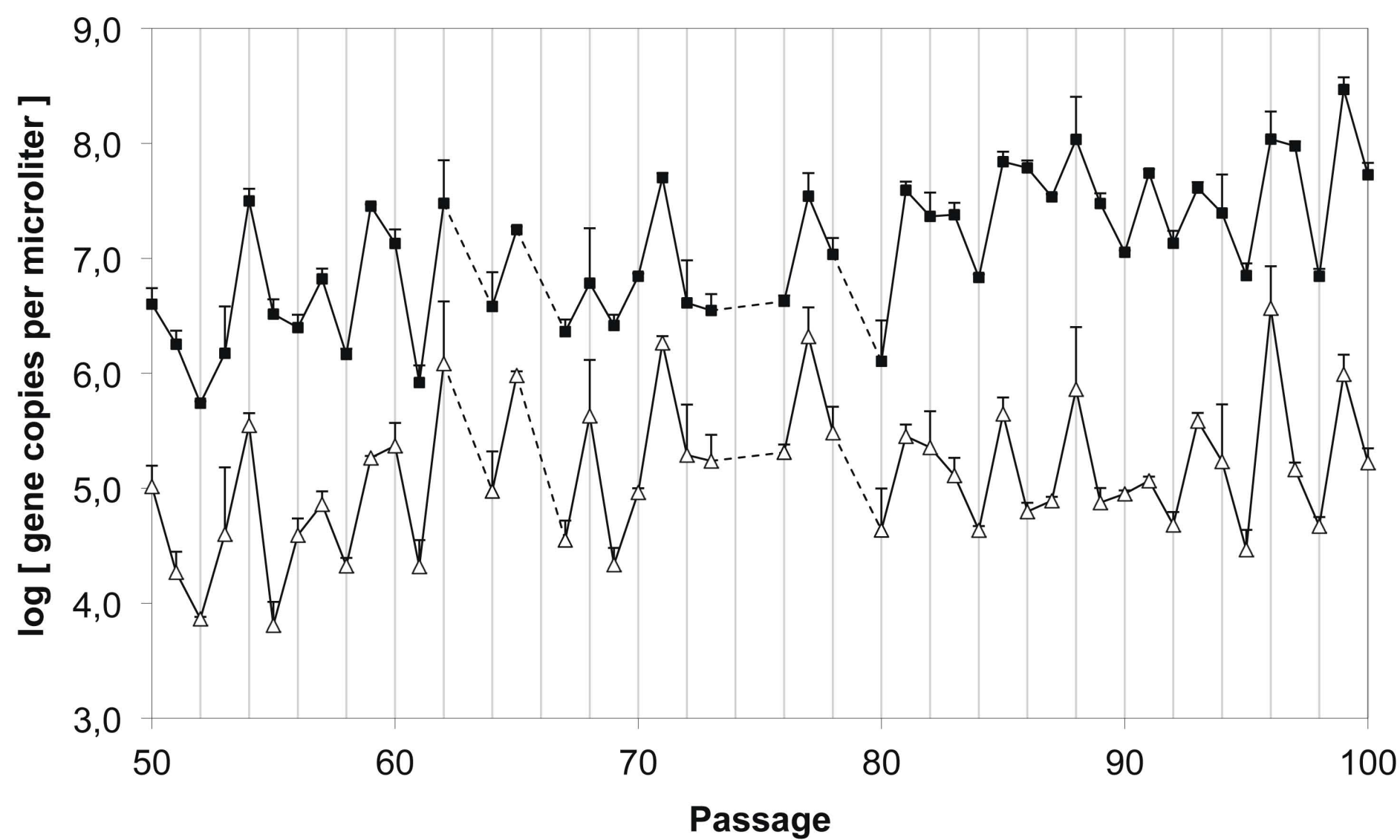
554 **Figure 4.** (a) Bifurcation diagram computed using the same parameter values as in the  
555 Figure 3e. However, here we show the dynamics as mutation is changed without  
556 considering stochastic effects (the mutation rate for each passage is  $\mu$ , and not a realization  
557 of  $\Omega$ ). The bifurcation diagram reveals a Ruelle-Takens-Newhouse (i.e., quasi-periodic)  
558 route to chaos at decreasing mutation rate, which is confirmed in the plot below. (b) Maximal  
559 Lyapunov exponent (MLE) for the same range of mutation rates shown in the bifurcation  
560 diagram above (the MLE is zero when a bifurcation takes place and positive when the  
561 dynamics is chaotic). After a first bifurcation (occurring at  $\mu \approx 0.9$ ), a series of flip bifurcations  
562 (within the range  $0.7 \leq \mu \leq 0.8$ ) take place indicating the quasi-periodic route to chaos.  
563 Then, some chaotic windows are identified by means of positive MLE (see horizontal dotted  
564 line at zero MLE values).

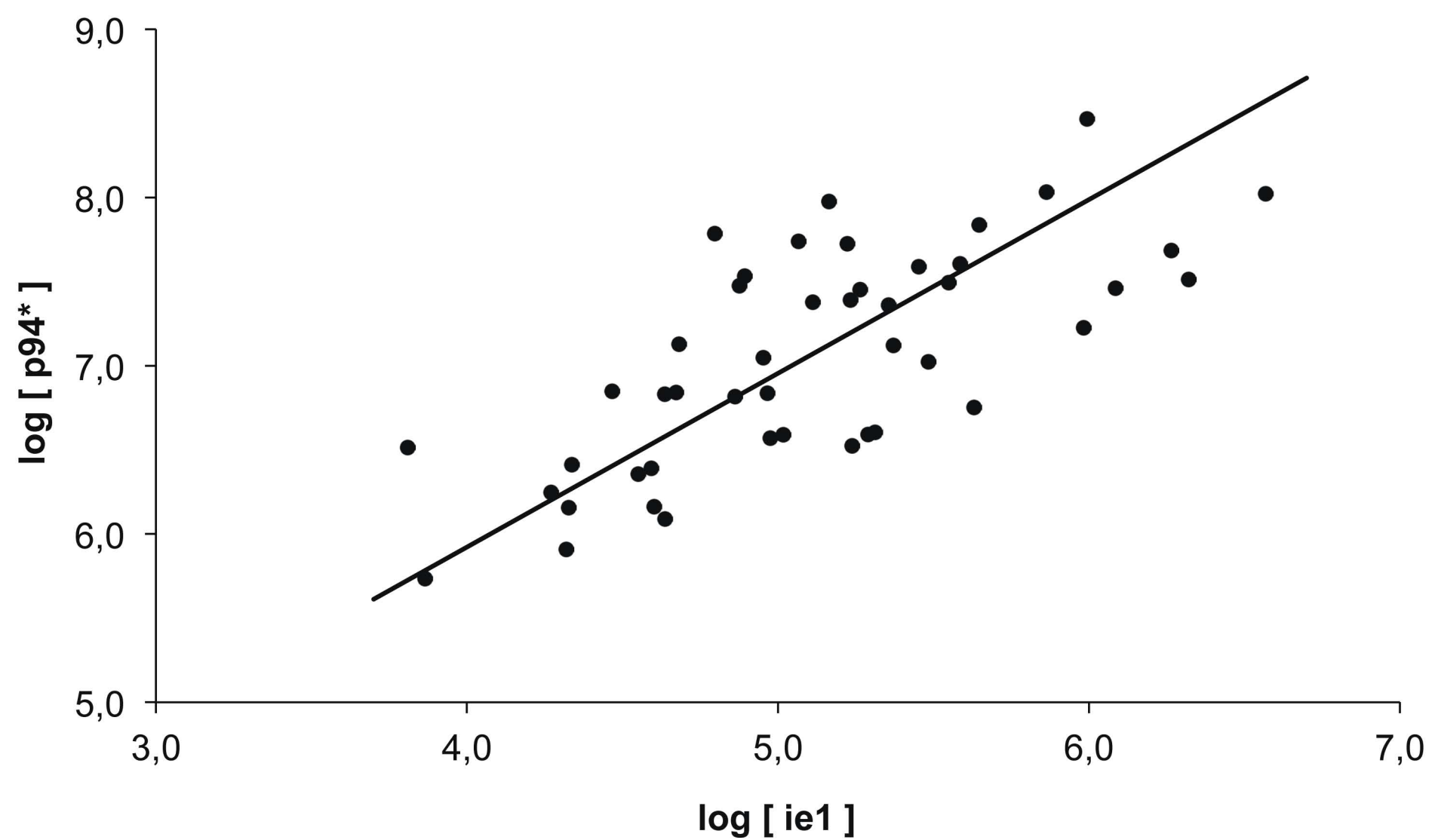
565

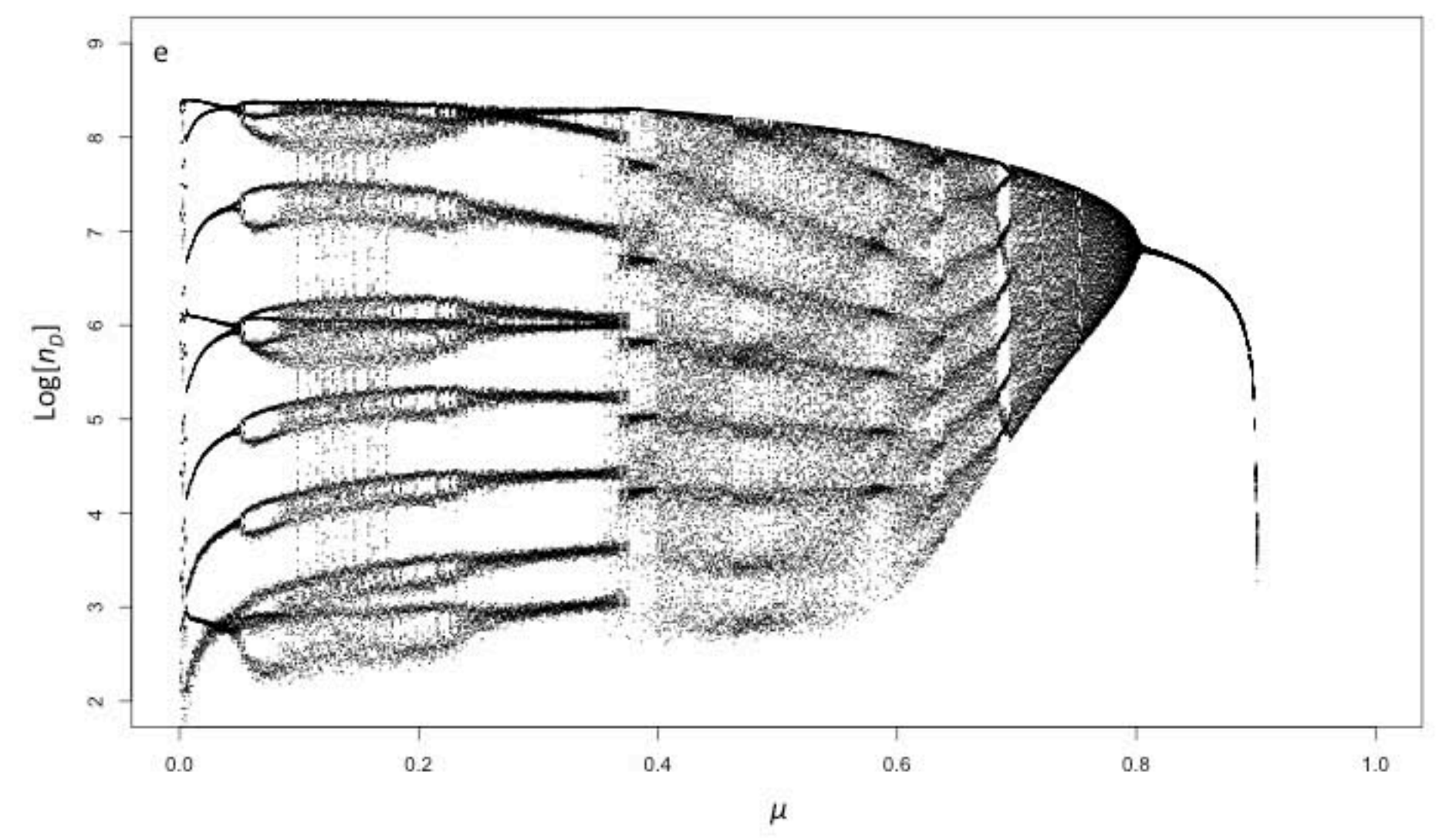
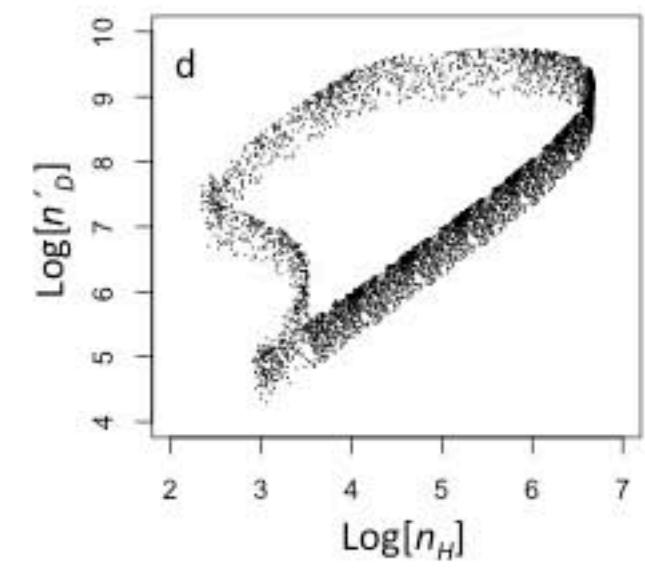
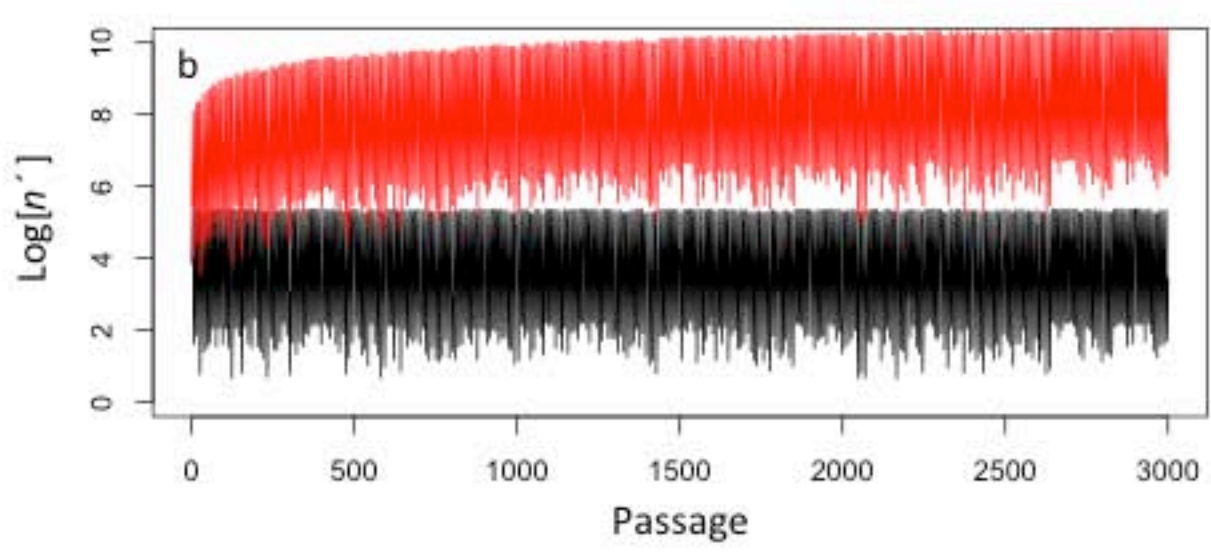
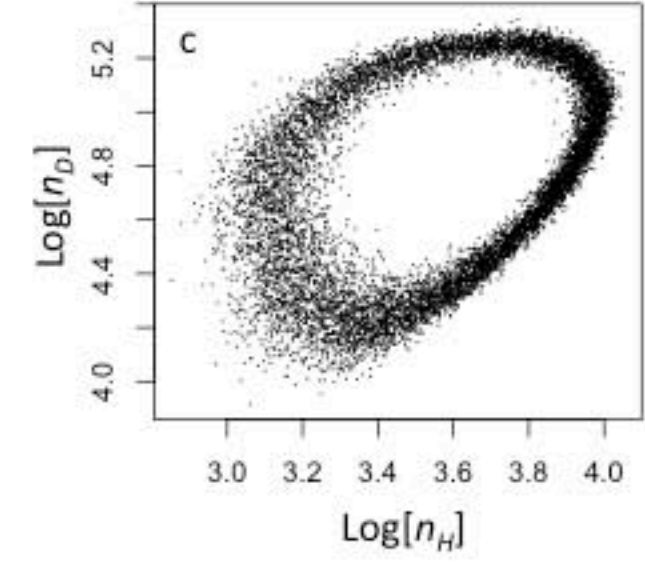
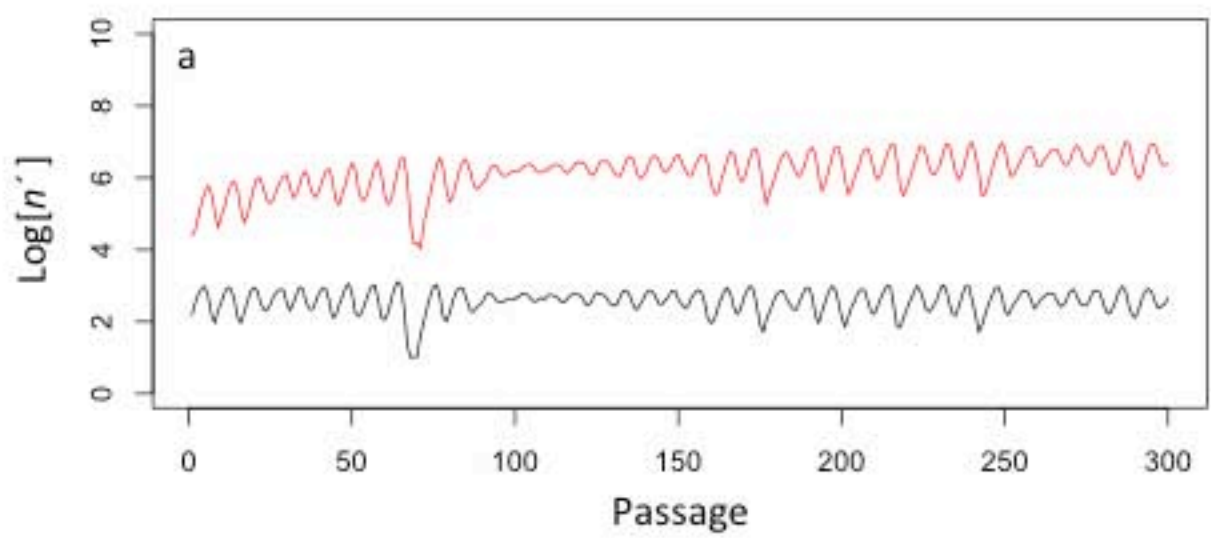
566 **Figure 5.** Predicted effects of experimental variation on the dynamics of virus populations.  
567 For all panels passage number is given on the abscissae, the log of the virus number is  
568 given on the ordinate and the trajectories of helper and DI viruses are given in black and red,

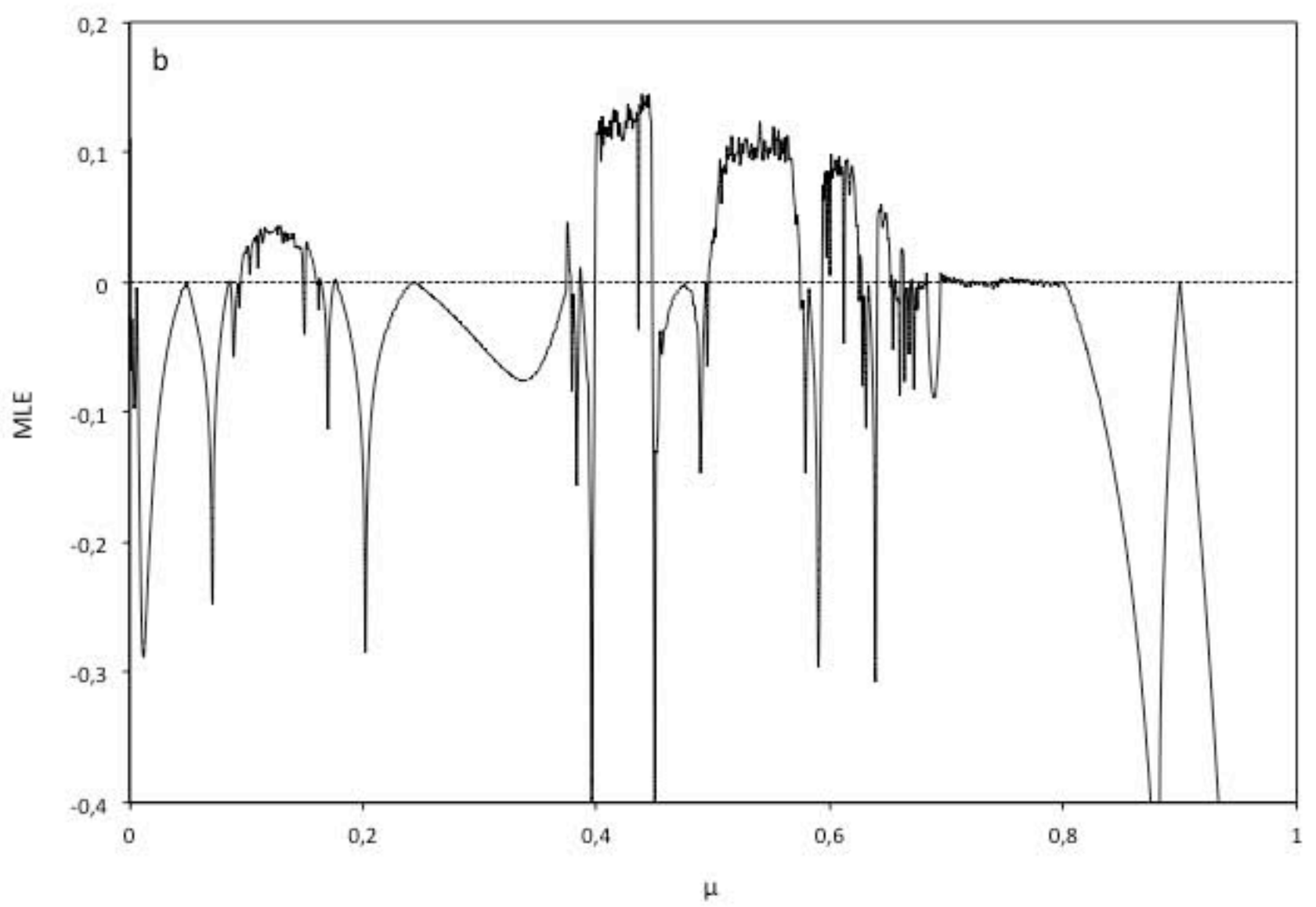
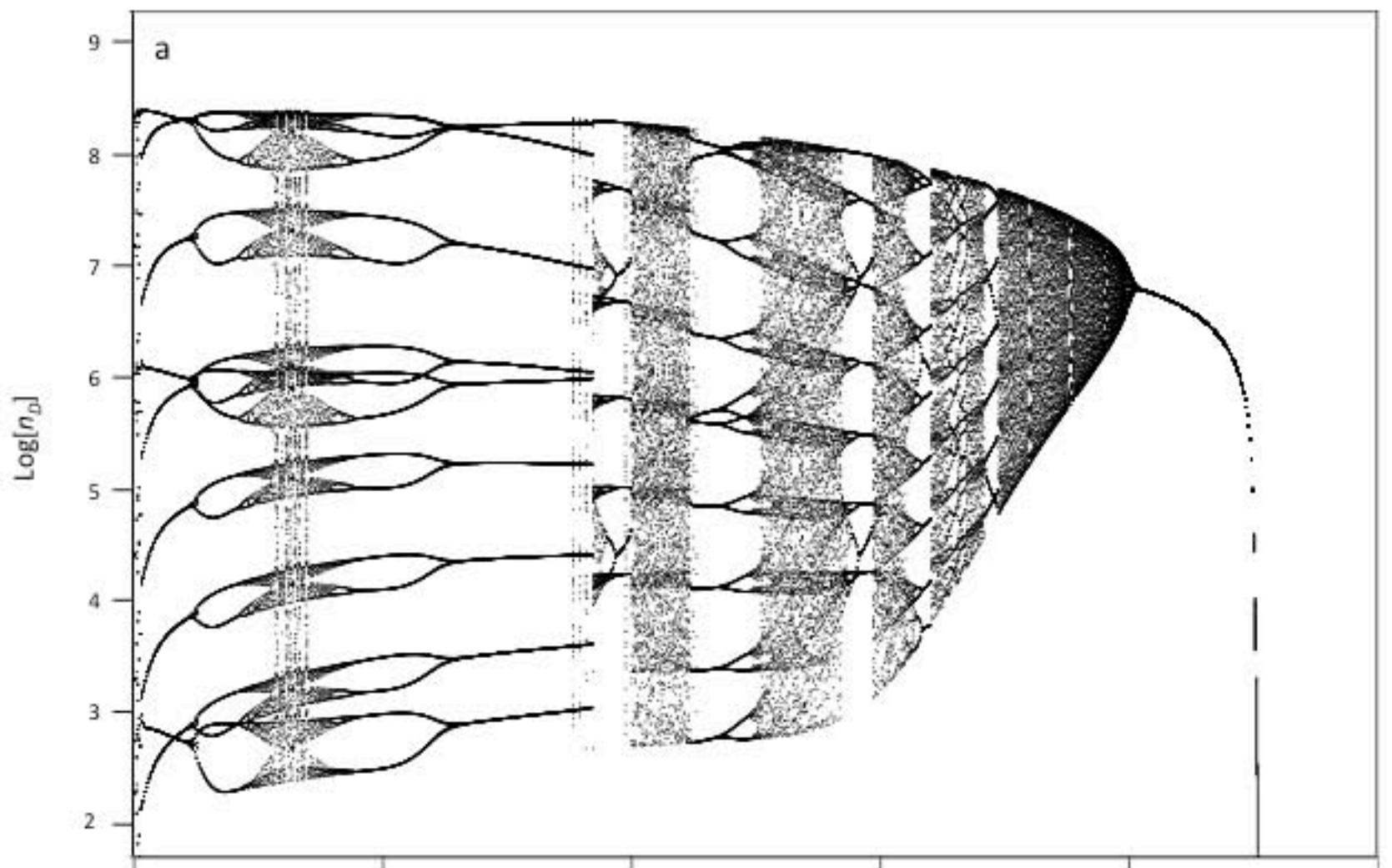


569 respectively. We considered the effects on model dynamics of two sources of stochasticity:  
570 (i) mutation, modeled as a binomially distributed number of cells in which the helper virus  
571 mutates to a DI virus, and (ii) variation in the number of cells over passages, modeled as a  
572 negative binomial distribution with  $p = 0.01$  and  $r = 5050.5$  resulting in a mean of  $5 \times 10^5$  and  
573 variance  $5 \times 10^7$ . We used the same model parameters as in Figure 3b ( $v_\alpha = 10$ ,  $v_\beta = 25$ ,  $\phi =$   
574  $0.0002$ ,  $c = 5 \times 10^5$ ), but set  $\xi = 0$  for clarity. For the left hand panels  $\mu = 0.35$ , resulting in an  
575 MLE well below zero ( $-0.068$ ; see Figure 4) and a two point cycle. For the right hand panels  
576  $\mu = 0.74$ , resulting in an MLE near zero ( $-0.005$ ) and a regular multipoint cycle. In panels (a)  
577 and (b), the results of the deterministic model are given. Here mutation has a fixed rate, and  
578 the number of cells is constant over passages. In panels (c) and (d), the number of cells is  
579 variable, following a binomial distribution over passages as described above. The effect is  
580 negligible when  $\mu = 0.35$  (c), but much stronger when  $\mu = 0.74$  (d). In panels (e) and (f),  
581 mutation is stochastic. The effects are stronger in panel (e) than in panel (f), because  
582 mutation follows a binomial distribution in which the number of trials is the number of cells  
583 infected only by the helper virus, and this number reaches lower levels in (e). The combined  
584 effects of stochastic mutation and a variable frequency of cells rendered similar results to  
585 that in panels e and f. These simulations reinforce the idea even if the deterministic model  
586 predicts non-chaotic dynamics for a particular set of parameters, experimental variation can  
587 generate time series with irregular fluctuations.









$\mu = 0.35$  $\mu = 0.74$ 